Enhanced surface melting of the Fennoscandian Ice Sheet during periods of North Atlantic cooling

Steven M. Boswell[1,2], Samuel Toucanne[3], Mathilde Pitel-Roudaut[3], Timothy T. Creyts[1], Frédérique Eynaud[4], Germain Bayon[3]

[1]*Lamont-Doherty Earth Observatory, Columbia University, Palisades, NY 10964, USA*

[2]*Department of Earth and Environmental Sciences, Columbia University, New York, NY 10027, USA*

[3]*IFREMER, Unité de Recherche Géosciences Marines, F-29280 Plouzané, France*

[4]*Laboratoire Environnements et Paléoenvironnements Océaniques et Continentaux (EPOC), UMR 5805, Université de Bordeaux, F-33615 Pessac, France*

ABSTRACT

Heinrich Events (HEs) are dramatic episodes of marine-terminating ice discharge and sediment rafting during periods of cold North Atlantic climate. However, the causal chain of events leading to their occurrence is unresolved. Here, we demonstrate that enhanced surface melting of land-terminating margins of the southern Fennoscandian Ice Sheet (FIS) is a recurring feature of Heinrich Stadials (HSs), the cold periods during which HEs occur. We use neodymium isotopes to show that the Channel River transported detrital sediments from the interior of eastern Europe to the Bay of Biscay in the Northeast Atlantic Ocean ca. 158 to 154 ka. Based on similar evidence from the last glacial period, we infer that this interval corresponds to the melting and retreat of the southern FIS margin despite contemporaneous cooling in the North Atlantic and central Europe. The FIS melting episode occurred just prior to a HE, consistent with

findings from the more recent HSs 1, 2, and 3. Based on this evidence, we clarify a sequence of events that precedes HEs. Precursor melting of North Atlantic-adjacent ice sheets induces an initial Atlantic meridional overturning circulation (AMOC) slowdown. Atmospheric changes during the resulting HS cause summertime warming in northern Europe that drives enhanced FIS melting. Subsequent meltwater discharge to the North Atlantic further weakens the AMOC and warms the intermediate water masses that contribute to HEs.

INTRODUCTION

The widespread melting of North (N.) Atlantic-adjacent ice sheets during periods of exceptionally cold polar climate is a paradoxical feature of recent glacial periods (e.g., Barker et al., 2015; Toucanne et al., 2015). Heinrich Events, in which armadas of icebergs discharge from marine-terminating ice margins into the N. Atlantic, punctuate the termination of cold Heinrich Stadials. HSs likely are caused by ocean surface cooling in response to freshwater-induced disruptions of the AMOC (e.g., Clark et al., 2007; Ivanovic et al., 2018). HEs then are triggered by the melting of marine-terminating grounded ice by the poleward transport of subsurface heat (700-1100 m depth, Alvarez-Solas et al., 2013) from low latitudes in response to further weakening of the AMOC (Shaffer et al., 2004; Marcott et al., 2011; Alvarez-Solas et al., 2013). However, the continental sources of freshwater that induce this AMOC destabilization during HSs remain debated.

During the last glacial period, HEs were preceded by the melting of terrestrial-terminating FIS margins. These FIS melting episodes, focused in the continental interior of Europe, lasted from the onset of HSs until the resulting HE as revealed by detailed study of HS1 (~18-15 ka), HS2 (~26-23 ka), and HS3 (~31-29 ka) (Toucanne et al., 2015). Here, we document sedimentary and geochemical evidence of terrestrial-terminating FIS margin melting during a period of extensive N. Atlantic cooling ca. 158-152 ka. Our results demonstrate that FIS melting during HSs precedes and contributes to the AMOC disruption that leads to HEs during both the last and penultimate glacial periods. Enhanced surface melting of the FIS prior to HEs is consistent with summertime warming in Europe during stadials (Schenk et al., 2018; Bromley et al., 2018).

Terminal moraines show that the British-Irish Ice Sheet (BIIS) and FIS coalesced in the North Sea ca. 160 ka during the Drenthe Stage of Marine Isotope Stage (MIS) 6 (Gibbard et al., 1988). When the BIIS and FIS coalesced, rivers of Britain, France, and the North European Plain (NEP; Fig. 1) integrated as tributaries of the Channel River, the sea level lowstand precursor of the modern English Channel (Fig. 1; Busschers et al., 2008). The Channel River drainage basin extended across much of northern Europe and drained large quantities of meltwater to the Bay of Biscay (e.g., Zaragosi et al., 2001; Toucanne et al., 2009, 2015). Sediments deposited off the Channel River mouth therefore record the timing and nature of ice sheet melting.

METHODS

FIS melting in the continental interior of Europe during MIS 6 is supported by the Nd isotopic composition of detrital sediments from Bay of Biscay core MD03-2692. This core is located in front of the former Channel River and records sedimentary discharge with high fidelity (Fig. 1; 46°49.72′ N, 9°30.97′ W, 4064 m; Eynaud et al., 2007). The Nd isotopic compositions of detrital sediments from the Channel River fingerprint their geographic origin within Europe (Toucanne et al., 2015). Following Toucanne et al. (2015), we determine that anomalously non-radiogenic Nd isotope signatures in the core sediments correspond to periods of southern FIS margin melting and retreat. To reconcile the Nd isotope signatures of the MD03-2692 sediments with their continental sources, we acquired Saalian (MIS 6-10) glacigenic sediments deposited by the Baltic Ice Stream in Denmark and Poland (Ehlers et al., 2011) (Fig. 1).

Nd isotope ratios were measured for the fine-fractions (<63 μm) of both the MD03-2692 core sediments (n=55; Table S1) and glacigenic sediments from the NEP (n=17; Table S2). We focus on the <63 μm fraction because the meltwaters from ice margins predominantly transport the clay and silt fractions of continental detritus (Brown and Kennett, 1998; Boswell et al., 2018). All samples were prepared per Bayon et al. (2002) prior to isolation of the Nd by ion-exchange chromatography. Nd isotope measurements were performed on a Thermo Scientific Neptune MC-ICP-MS at the Pôle Spectrométrie Océan, France, using a sample-standard bracketing method. Procedural Nd blanks were negligible compared to the amount of Nd in the studied samples. We estimate the 2σ uncertainty of our measurements to be ±0.3 ε-units based on replicate analyses of the JNdi-1 standard solution ($^{143}Nd/^{144}Nd = 0.512115 \pm 0.000009$, 2σ, n=31). We report $^{143}Nd/^{144}Nd$ ratios in εNd notation, $[(^{143}Nd/^{144}Nd)_{sample}/(^{143}Nd/^{144}Nd)_{CHUR} - 1] \times 10^4$, using the $(^{143}Nd/^{144}Nd)_{CHUR}$ value of 0.512638 (Jacobsen and Wasserburg, 1980).

The MIS 6 chronology for MD03-2692 (Table S3) is constructed by tuning the abundances of the polar planktic foraminifera *N. pachyderma* (s.s. sinistral) in the core to those from the ODP 983 core (Barker et al., 2015) that has been recently synchronized to the synthetic Greenland ‘Speleo-Age’, a U-Th based chronology (Barker et al., 2011). The dominance of *N. pachyderma* in the sediments corresponds to periods of intense cooling, and we presume that the onset of these cold periods, interpreted to represent the southward migration of the polar front, is concurrent across the N. Atlantic (Barker et al., 2015). From this initial chronology, we observe that the high-resolution Ca/Fe ratios of MD03-2692 sediments, reflecting climatically-driven biogenic carbonate fluxes, are closely aligned with the synthetic Greenland temperatures (GL_T_syn) of Barker et al. (2011). This coupling of Ca/Fe ratios and GL_T_syn allows us to fine-tune the final age model (e.g., Hodell et al., 2013) (Table S3; Fig. S1).

LINKING BALTIC SEDIMENT TO SOUTHERN FIS MARGIN RETREAT

Throughout most of MIS 6, the εNd values of the core sediments vary between -10.8 and -12.0 (Fig. 2F). These values are consistent with downstream Channel River sources (e.g., Ireland, Great Britain, and France), including the BIIS (Toucanne et al., 2015). As inferred from the radiogenic Nd signatures and two-fold increase in mass accumulation rate (MAR) of detrital sediments at the core site (Fig. 2F, G), enhanced melting of the BIIS began ca. 160 ka. However, the εNd of the core sediments from 158 to 154 ka reached values of -14.0 (Fig. 2F), revealing that the dominant portion of Channel River sediments were sourced from the eastern NEP (-14.4) by 156 ka. This Baltic sediment provenance demonstrates that the southern margin of the FIS was melting, retreating, and dispatching large quantities of sediment to the Channel River (Fig. 2F, G). Benthic foraminifera record an ~12 m sea level equivalent (SLE) reduction in the size of global ice sheets ca. 159 to 156 ka (Fig. 2A; Waelbroeck et al., 2002). This ice volume decrease is synchronous with a substantial retreat of the southern FIS margin from the Drenthe maximum to a spatial extent even more restricted than the subsequent Warthe limits (Fig. 1; Toucanne et al., 2009). Considering the size of the FIS ca. 160 ka (~60 m SLE, Lambeck et al., 2006), a large volume of FIS meltwater was discharged through the Channel River (Fig. 2F). The corresponding increase in Channel River flow led to greater volumes of anchor ice (from wintertime freezing of the river bed) that were transported to the Bay of Biscay during the spring thaw (Toucanne et al., 2009). In total, the melting episode resulted in a 2.5 m section of seasonally laminated IRD termed ‘Channel River IRD’ and massive muds in the deep Bay of Biscay (Fig. 2E, G). This accumulation is 1.5 times greater than at Termination I (ca. 18-17 ka, Zaragosi et al., 2001).

To verify that the ca. 156 ka event reflects FIS margin melting, we draw on evidence from the last glacial period. Terrestrial-based paleogeographical reconstructions of the FIS (Hughes et al., 2016) reveal that the southern FIS margins retreated in phase with Channel River discharge events identified during HS1, HS2, and HS3 (Fig. 3). Based on the similarity of sedimentary and geochemical evidence, we infer that the terrestrial-terminating FIS margin was melting and retreating from ~158 to 154 ka (Fig. 2A, F, G).

ICE SHEET MELTING AND AMOC SLOWDOWN DURING STADIALS

FIS melting in the continental interior ca. 158-154 ka occurs during a period of cooling that extends from ~158-152 ka in the N. Atlantic and central Europe. The cooling interval is inferred from the relative abundances of *N. pachyderma* in sediments from cores ODP 983 and MD03-2692 (Barker et al., 2015; Eynaud et al., 2007) and the $\delta^{18}O$ of cave flowstones (Fig. 2B, C; Koltai et al., 2017). The onset of southeastern FIS melting leads to the export of cold FIS meltwaters to the Bay of Biscay and Portuguese coast, deduced from both increased concentrations of freshwater *Pediastrum* and pre-Quaternary dinocyst algae in MD03-2692 core sediments (Fig. 2F; Eynaud et al., 2007; Penaud et al., 2009) and increased proportions of tetra-unsaturated alkenones (C37:4%) in the surface waters above the MD01-2444 core site (Fig. 2C; Margari et al., 2014).

FIS melting, and the corresponding flux of freshwater to the open ocean, precedes AMOC disruption (Fig. 2D) and an increase in IRD deposition across the central and eastern N.

Atlantic ~155-154 ka (Fig. 2E). The AMOC is sensitive to freshwater discharge to the Northeast Atlantic (Roche et al., 2010), a focal point of FIS meltwater routing. Because the FIS was more voluminous ca. 155 ka than at the LGM (e.g., Fig. 1; Ehlers et al., 2011), enhanced FIS melting likely contributed to AMOC disruption (e.g., Ivanovic et al., 2018). While the strength of the AMOC was reduced during the entire HS (i.e., decreased $\delta^{13}C$ of benthic foraminifera in core ODP 983; Barker et al., 2015), the precipitous decline in AMOC strength ~155-154 ka is coeval with the widespread deposition of IRD (Fig. 2D, E). Although the provenance of the IRD deposited ~155 ka is uncertain, the N. Atlantic stadial bracketing the FIS melting interval is analogous to HS1, HS2, and HS3 in that melting of the terrestrial-terminating ice sheet (TIS) margins in Europe preceded calving of marine-terminating ice sheet (MIS) margins in the N. Atlantic region (Fig. 2).

ENHANCED SURFACE MELTING OF THE FIS DURING N. ATLANTIC STADIALS

The coalescence of grounded FIS and BIIS margins in the North Sea (Fig. 1) precludes an ocean warming trigger for terrestrial-terminating FIS margin retreat in the European interior between 158 and 154 ka. Therefore, FIS melting in the Baltic lowlands likely results from an increase in summertime temperatures. Summer insolation rise (Fig. 2G) is relatively muted during the studied interval, however, suggesting the possible influence of an internal climate feedback. Reductions in subpolar N. Atlantic temperatures during spring and autumn, as indicated by *N. pachyderma* abundances (Fig. 2B; Jonkers and Kučera, 2015), do not preclude heightened seasonality such as increased summer temperatures in the N. Atlantic and Europe. High-resolution climate simulations and proxy evidence, including the disintegration of the Scottish ice cap, support the occurrence of warm European summers during the Younger Dryas stadial (Schenk et al., 2018; Bromley et al., 2018). Although increased aridity could partially explain FIS margin retreat and melting via reduced snow accumulation and increased albedo (i.e., ‘dirty ice’) at the FIS surface, such evidence is presently lacking.

Warm European summers in response to ocean cooling (e.g., Schenk et al., 2018; Bromley et al., 2018) are likely a recurring feature of N. Atlantic stadials. During MIS 6, precursor discharge of meltwaters to the N. Atlantic ca. 160 ka, including from European ice sheets (Fig. 2G), is consistent with an initial disruption of the AMOC (Fig. 2D) and the onset of cooling in the N. Atlantic and mainland Europe (Fig. 2B, C) (e.g., Clark et al., 2007; Ivanovic et al., 2018). FIS melting in the continental interior increased, however, ca. 158-154 ka when central European and N. Atlantic surface temperatures were coldest (Fig. 2C, F). Atmospheric blocking (e.g., Schenk et al., 2018) during HS summers explains the apparent contradiction of ice sheet surface melting in northern Europe while the subpolar N. Atlantic and Europe cool in unison (Fig. 2B, C; Barker et al., 2015; Koltai et al., 2017). During HSs, the flux of FIS meltwaters to the N. Atlantic results in a cold, low-salinity ocean surface that aids the growth of sea ice and likely contributes to the ocean cooling-N. European warming feedback (e.g., Schenk et al., 2018). Increased density stratification in the water column causes the AMOC to slow down further (~155 ka) (e.g., Clark et al., 2007; Fig. 2D). Eventually, AMOC disruption induces the subsurface ocean warming (Shaffer et al., 2004) that melts the marine-terminating grounded ice of the LIS and other N. Atlantic-adjacent ice sheets, leading to enhanced ice discharge to the ocean as HEs (Fig. 2D, E; Alvarez-Solas et al., 2013). Lags between summertime warming in Europe and the onset of HEs are consistent with FIS melting prior to the widespread deposition of IRD across the N. Atlantic during HSs of both the last glacial period (Zaragosi et al., 2001; Toucanne et al., 2015) and the stadial from 158 to 152 ka (Fig. 2E, F).

Lastly, we consider the possibility that summertime warming during stadials extends beyond Europe. We note, for instance, that warming in Antarctica is concurrent with HSs (e.g., EPICA Community Members, 2006; Clark et al., 2007) and thus FIS melting. Nonetheless, conceptualizing N. Atlantic stadials as intervals of increased seasonality and regional summer warming during periods of mean cooling (e.g., Denton et al., 2005; Schenk et al., 2018) resolves the apparent contradiction between cold N. Atlantic climates and contemporaneous melting of land-terminating ice sheet margins in Europe. Consistent with the temporal relationships between the onset of FIS melting, AMOC destabilization, and HEs during the past two glacial periods, warm European summers are a regular feature of HSs and contribute to the enhanced FIS surface melting that precedes HEs.

ACKNOWLEDGMENTS

Glacigenic sediments from Poland were graciously supplied by D. Krzyszkowski. A. de Prunelé provided technical assistance with ICP-MS analyses. The authors are grateful to G. Denton and G. Soulet for providing feedback on this manuscript. This study was made possible by financial support from the Office for Science and Technology of the Embassy of France in the United States. TTC was supported by a Vetlesen Foundation grant, NSF-1643970, and NASA-NNX16AJ95G.

REFERENCES CITED

Alvarez-Solas, J., Robinson, A., Montoya, M., and Ritz, C., 2013, Iceberg discharges of the last glacial period driven by oceanic circulation changes: Proceedings of the National Academy of Sciences, v. 110, no. 41, p. 16350-16354, doi: 10.1073/pnas.1306622110

Barker, S., Knorr, G., Edwards, R.L., Parrenin, F., Putnam, A.E., Skinner, L.C., Wolff, E., and Ziegler, M., 2011, 800,000 years of abrupt climate variability: Science, v. 334, no. 6054, p. 347-351, doi: 10.1126/science.1203580

Barker, S., Chen, James, Gong, Xun, Jonkers, L., Knorr, G., and Thornalley, D., 2015, Icebergs not the trigger for North Atlantic cold events: Nature, v. 520, no. 7547, p. 333-336, doi: 10.1038/nature14330

Bayon, G., German, C.R., Boella, R.M., Milton, J.A., Taylor, R.N., and Nesbitt, R.W., 2002, An improved method for extracting marine sediment fractions and its application to Sr and Nd isotopic analysis: Chemical Geology, v. 187, no. 3, p. 179-199, doi: https://doi.org/10.1016/S0009-2541(01)00416-8

Bromley, G., Putnam, A., Borns Jr, H., Lowell, T., Sandford, T., and Barrell, D., 2018, Interstadial rise and Younger Dryas demise of Scotland's last ice fields: Paleoceanography and Paleoclimatology, v. 33, no. 4, p. 412-429, doi: 10.1002/2018PA003341

Brown, P.A., and Kennett, J.P., 1998, Megaflood erosion and meltwater plumbing changes during last North American deglaciation recorded in Gulf of Mexico sediments: Geology, v. 26, no. 7, p. 599-602, doi: https://doi.org/10.1130/0091-7613(1998)026<0599:MEAMPC>2.3.CO;2

Boswell, S.M., Toucanne, S., Creyts, T.T., and Hemming, S.R., 2018, Continental-scale transport of sediments by the Baltic Ice Stream elucidated by coupled grain size and Nd provenance analyses: Earth and Planetary Science Letters, v. 490, p. 143-150, doi: https://doi.org/10.1016/j.epsl.2018.03.017

Busschers, F.S., Van Balen, R.T., Cohen, K.M., Kasse, C., Weerts, H.J., Wallinga, J., and Bunnik, F.P., 2008, Response of the Rhine–Meuse fluvial system to Saalian ice-sheet dynamics: Boreas, v. 37, no. 3, p. 377-398. doi: 10.1111/j.1502-3885.2008.00025.x

Clark, P.U., Hostetler, S.W., Pisias, N.G., Schmittner, A. and Meissner, K.J., 2007, Mechanisms for an ~7-kyr Climate and Sea-Level Oscillation during Marine Isotope Stage 3, *in* Schmittner, A., Chiang, J., and Hemming, S., eds., Ocean Circulation: Mechanisms and Impacts: AGU, Washington, D.C., Geophysical Monograph Series vol. 173, p. 209-246, doi: https://doi.org/10.1029/173GM15

Denton, G.H., Alley, R.B., Comer, G.C., and Broecker, W.S., 2005, The role of seasonality in abrupt climate change: Quaternary Science Reviews, v. 24, no. 10-11, p. 1159-1182, doi: https://doi.org/10.1016/j.quascirev.2004.12.002

Ehlers, J., Gibbard, P.L., and Hughes, P.D., 2011. Quaternary Glaciations – Extent and Chronology, v. 15, p. 1126, Elsevier, Amsterdam

EPICA Community Members, 2006, One-to-one coupling of glacial climate variability in Greenland and Antarctica: Nature, v. 444, p. 195–198, doi: doi:10.1038/nature05301

Eynaud, F., Zaragosi, S., Scourse, J.D., Mojtahid, M., Bourillet, J.F., Hall, I.R., Penaud, A., Locascio, M., and Reijonen, A., 2007, Deglacial laminated facies on the NW European continental margin: The hydrographic significance of British-Irish Ice Sheet deglaciation and Fleuve Manche paleoriver discharges: Geochemistry, Geophysics, Geosystems, v. 8, no. 6, doi: 10.1029/2006GC001496

Gibbard, P.L., 1988, The history of the great northwest European rivers during the past three million years: Royal Society of London Philosophical Transactions, ser. B, v. 318, no. 1191, p. 559-602, doi: 10.1098/rstb.1988.0024

Hodell, D., Crowhurst, S., Skinner, L., Tzedakis, P.C., Margari, V., Channell, J.E., Kamenov, G., Maclachlan, S., and Rothwell, G., 2013, Response of Iberian Margin sediments to orbital and suborbital forcing over the past 420 ka: Paleoceanography, v. 28, no. 1, p. 185-199, doi: https://doi.org/10.1002/palo.20017

Hughes, A.L., Gyllencreutz, R., Lohne, Ø.S., Mangerud, J., and Svendsen, J.I., 2015, The last Eurasian ice sheets–a chronological database and time-slice reconstruction, DATED-1: Boreas, v. 45, no. 1, p. 1-45, doi: 10.1111/bor.12142.

Ivanovic, R.F., et al., 2018, Acceleration of northern ice sheet melt induces AMOC slowdown and northern cooling in simulations of the early last deglaciation: Paleoceanography and Paleoclimatology, doi: https://doi.org/10.1029/2017PA003308

Jacobsen, S.B., and Wasserburg, G.J., 1980, Sm-Nd isotopic evolution of chondrites: Earth and Planetary Science Letters, v. 50, no. 1, p. 139-155, doi: https://doi.org/10.1016/0012-821X(80)90125-9

Jonkers, L., and Kučera, M., 2015, Global analysis of seasonality in the shell flux of extant planktonic Foraminifera, Biogeosciences, v. 12, no. 7, p. 2207-2226, doi: https://doi.org/10.5194/bg-12-2207-2015

Koltai, G., Spötl, C., Shen, C.C., Wu, C.C., Rao, Z., Palcsu, L., Kele, S., Surányi, G., and Bárány-Kevei, I., 2017, A penultimate glacial climate record from southern Hungary: Journal of Quaternary Science, v. 32, no. 7, p. 946-956, doi: https://doi.org/10.1002/jqs.2968

Laskar, J., Robutel, P., Joutel, F., Gastineau, M., Correia, A.C.M., and Levrard, B., 2004. A long-term numerical solution for the insolation quantities of the Earth: Astronomy & Astrophysics, v. 428, no. 1, p. 261-285, doi: https://doi.org/10.1051/0004-6361:20041335

Lambeck, K., Purcell, A., Funder, S., Kjær, K., Larsen, E., and Moller, P.E.R., 2006, Constraints on the Late Saalian to early Middle Weichselian ice sheet of Eurasia from field data and rebound modelling: Boreas, v. 35, no. 3, p. 539-575, doi: 10.1080/03009480600781875

Marcott, S.A., et al., 2011, Ice-shelf collapse from subsurface warming as a trigger for Heinrich events: Proceedings of the National Academy of Sciences, v. 108, no. 33, p. 13415-13419, doi: 10.1073/pnas.1104772108

Margari, V., Skinner, L.C., Hodell, D.A., Martrat, B., Toucanne, S., Grimalt, J.O., Gibbard, P.L., Lunkka, J.P., and Tzedakis, P.C., 2014, Land-ocean changes on orbital and millennial time scales and the penultimate glaciation: Geology, v. 42, no. 3, p. 183-186, doi: https://doi.org/10.1130/G35070.1

Penaud, A., Eynaud, F., Turon, J.L., Zaragosi, S., Malaizé, B., Toucanne, S., and Bourillet, J.F., 2009, What forced the collapse of European ice sheets during the last two glacial periods (150 ka B.P. and 18 ka cal B.P.)? Palynological evidence: Palaeogeography, Palaeoclimatology, Palaeoecology, v. 281, no. 1-2, p. 66-78. doi: https://doi.org/10.1016/j.palaeo.2009.07.012

Roche, D.M., Wiersma, A.P., and Renssen, H., 2010, A systematic study of the impact of freshwater pulses with respect to different geographical locations: Climate Dynamics, v. 34, no. 7-8, p. 997-1013, doi: https://doi.org/10.1007/s00382-009-0578-8

Schenk, F., Väliranta, M., Muschitiello, F., Tarasov, L., Heikkilä, M., Björck, S., Brandefelt, J., Johansson, A.V., Näslund, J.O., and Wohlfarth, B., 2018, Warm summers during the Younger Dryas cold reversal: Nature Communications, v. 9, doi: 10.1038/s41467-018-04071-5

Shaffer, G., Olsen, S. M., and Bjerrum, C. J., 2004, Ocean subsurface warming as a mechanism for coupling Dansgaard-Oeschger climate cycles and ice-rafting events: Geophysical Research Letters, v. 31, no. 24, doi: 10.1029/2004GL020968

Toucanne, S., et al., 2009, Timing of massive 'Fleuve Manche' discharges over the last 350kyr: insights into the European ice-sheet oscillations and the European drainage network from MIS 10 to 2: Quaternary Science Reviews, v. 28, no. 13, p. 1238-1256, doi: https://doi.org/10.1016/j.quascirev.2009.01.006

Toucanne, S., Soulet, G., Freslon, N., Jacinto, R.S., Dennielou, B., Zaragosi, S., Eynaud, F., Bourillet, J.F., and Bayon, G., 2015, Millennial-scale fluctuations of the European Ice Sheet at the end of the last glacial, and their potential impact on global climate: Quaternary Science Reviews, v. 123, p. 113-133, doi: http://dx.doi.org/10.1016/j.quascirev.2015.06.010

Waelbroeck, C., Labeyrie, L., Michel, E., Duplessy, J.C., McManus, J.F., Lambeck, K., Balbon, E., and Labracherie, M., 2002, Sea-level and deep water temperature changes derived from benthic foraminifera isotopic records: Quaternary Science Reviews, v. 21, no. 1, p. 295-305, doi: https://doi.org/10.1016/S0277-3791(01)00101-9

Weatherall, P., Marks, K.M., Jakobsson, M., Schmitt, T., Tani, S., Arndt, J.E., Rovere, M., Chayes, D., Ferrini, V., and Wigley, R., 2015, A new digital bathymetric model of the world's oceans: Earth and Space Science, v. 2, no. 8, p. 331-345, doi: https://doi.org/10.1002/2015EA000107

Zaragosi, S., Eynaud, F., Pujol, C., Auffret, G.A., Turon, J.L., and Garlan, T., 2001, Initiation of the European deglaciation as recorded in the northwestern Bay of Biscay slope environments (Meriadzek Terrace and Trevelyan Escarpment): a multi-proxy approach:

Earth and Planetary Science Letters, v. 188, no. 3, p. 493-507, doi: https://doi.org/10.1016/S0012-821X(01)00332-6

FIGURE CAPTIONS

Figure 1. An overview of the core sites, locales, and ice sheets discussed in this manuscript. The terminal limits of the Fennoscandian Ice Sheet (FIS) during the Drenthe Stage ('D', MIS 6; Ehlers et al., 2011) are outlined in bold. For comparison, FIS limits during the Warthe Stage ('W', MIS 6) and Last Glacial Maximum ('LGM'; Hughes et al., 2016) are shown as long and short dashed lines, respectively. The Channel River (blue) transports freshwater and terrigenous sediment from the North European Plain (NEP) to the N. Atlantic. Glacigenic sediments (Table S2) were sampled from sites (red dots) in Denmark and Poland. Blue lines in the N. Atlantic correspond to transport pathways for ice-rafted detritus (IRD; Barker et al., 2015).

Figure 2. Paleoenvironmental proxies record melting of the terrestrial-terminating ice stream (TIS) of the Fennoscandian Ice Sheet (FIS) prior to the calving of marine-terminating ice streams (MIS) during a Heinrich Stadial (HS) highlighted in the vertical gray bar. (A) Synthetic Greenland temperatures with orbital components (GL_T_syn, purple curve; Barker et al., 2011) and relative sea level (RSL, gray curve; Waelbroeck et al., 2002). (B) Relative abundances of the planktic foraminifera *N. pachyderma* in cores MD03-2692 (purple; Eynaud et al., 2007) and ODP 983 (blue; Barker et al., 2015). (C) $\delta^{18}O$ of Abaliget Cave, Hungary (pink and dark gray; Koltai et al., 2017) and alkenone SST from Portuguese margin core MD01-2444 (light gray; Margari et al., 2014). (D) $\delta^{13}C$ of benthic foraminifera from ODP 983 (Barker et al., 2015). (E) Normalized counts of ice-rafted detritus (IRD) from ODP 983 (black; Barker et al., 2015) and

MD03-2692 (orange; Eynaud et al., 2007). Channel River IRD supplied locally to the MD03-2692 core site (e.g., Toucanne et al., 2009), but not to the central Atlantic, from ~158 to 156 ka. (F) ε-Neodymium of sediments in core MD03-2692 (red) (Table S1). εNd values less than -12.4 reflect a southern FIS sediment provenance, but εNd values greater than -12.4 indicate a western European origin (Table S2; e.g., Toucanne et al., 2015). “P” (-14.4±0.7) and “D” (-12.4±0.3) εNd values (2σ) correspond to the mean signatures of Saalian glacigenic moraine sediment from Poland and Denmark (Table S2), respectively. Concentrations of freshwater *Pediastrum* and pre-Quaternary dinocyst algae are given by the light and dark blue lines, respectively (Eynaud et al., 2007; Penaud et al., 2009). (G) Mass accumulation rate (MAR) for sediments in core MD03-2692 (black; Table S4). A 2 kyr moving average was applied to the linearly interpolated terrigenous flux data. Insolation for June 21 at 55°N (orange; Laskar et al., 2004). Tie points for the MD03-2692 core chronology are designated by triangles (see the GSA Data Repository for details). All proxies are on the ‘Speleo-Age’ timescale (Barker et al., 2011) except the Abaliget Cave record and RSL estimates.

Figure 3. Paleogeography of western Europe, including the Channel River hydrographic network and the glacial limits of the Fennoscandian (FIS) and British-Irish Ice Sheets (BIIS) shown in snapshots covering the ca. 32-17 ka time interval (Hughes et al., 2016). These snapshots highlight the relationship between ice-marginal fluctuations of the FIS (Hughes et al., 2016) and Channel River runoff in the Bay of Biscay (Toucanne et al., 2015). Retreating FIS margins that contribute meltwater to the Channel River are outlined in red. High runoff (R) events occurred throughout or during Heinrich Stadials (HS) 3 (~32-29 ka), 2 (~26-23.5 ka) and 1 (~18-15 ka) as recorded at site MD95-2002 (Toucanne et al., 2015). These R events resulted from substantial

melting and retreat of southern FIS margins (Hughes et al., 2016). Ice advance in the continental interior and the North European Plain (NEP) is coeval with decreased runoff of the Channel River during the intervals between these HSs (i.e., Greenland Interstadial 3/4 and the global Last Glacial Maximum). The retreat and advance of ice margins between time slices is shown by yellow and blue highlighting, respectively (modified from Hughes et al., 2016). Dashed lines at the Channel River mouth document the coastline at the global Last Glacial Maximum, when the sea level was ~120 m lower than at present (Waelbroeck et al., 2002). The possible routing of FIS meltwater to the Nordic Seas (i.e., ice-free conditions in the North Sea) is indicated by the ‘?’ symbol. All data, including the GEBCO_2014 grid (Weatherall et al., 2015), are shown using a WGS 1984 North Pole Lambert Azimuthal Equal Area projection.

[1]GSA Data Repository item 201Xxxx, Tables S1-S4 and Figure S1, is available online at www.geosociety.org/pubs/ft20XX.htm, or on request from editing@geosociety.org

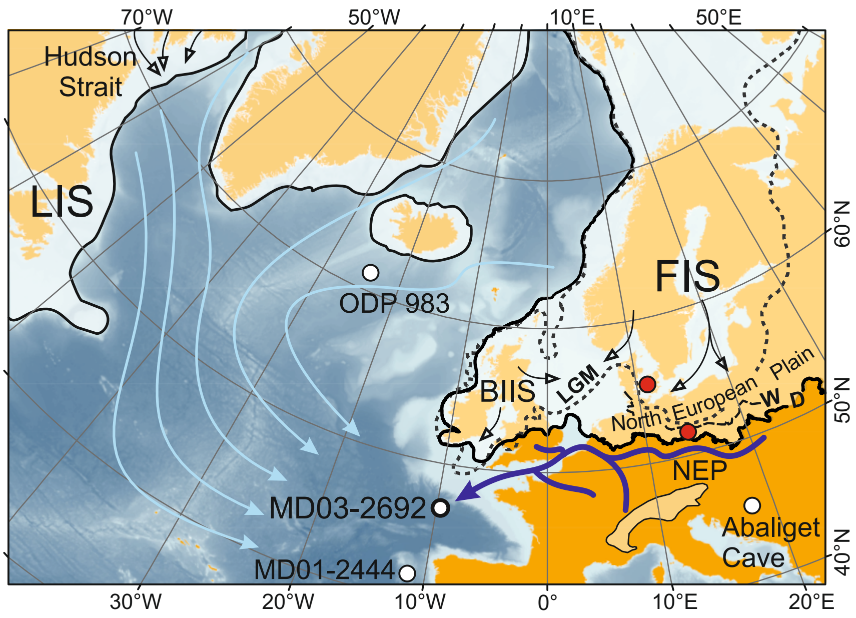
70°W
50°W
10°E
50°E
Hudson
Strait
LIS
ODP 983
FIS
BIIS
LGM
North European Plain
W
D
NEP
MD03-2692
Abaliget
Cave
MD01-2444
60°N
50°N
40°N
30°W
20°W
10°W
0°
10°E
20°E

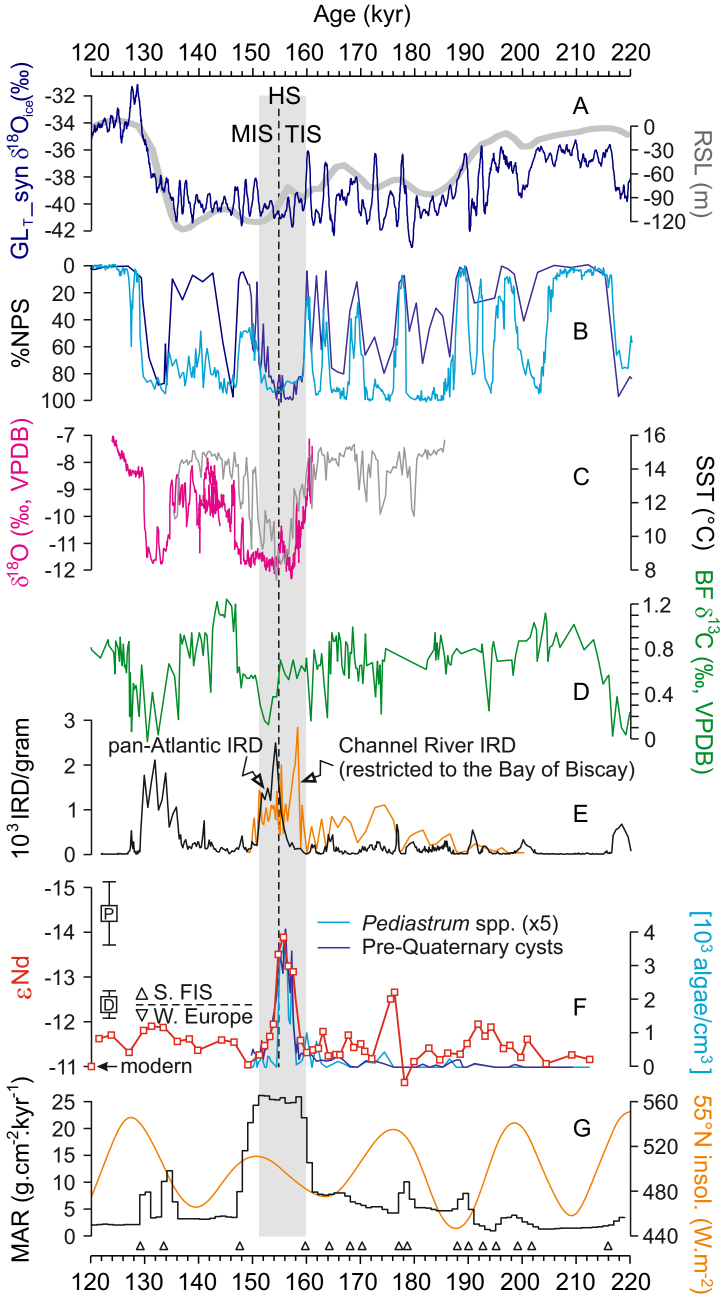

Age (kyr)
120 130 140 150 160 170 180 190 200 210 220
A
HS
MIS TIS
$GL_{T\_}syn\ \delta^{18}O_{ice}$(‰)
RSL (m)
B
%NPS
C
$\delta^{18}O$ (‰, VPDB)
SST (°C)
D
BF $\delta^{13}C$ (‰, VPDB)
E
10^3 IRD/gram
pan-Atlantic IRD
Channel River IRD
(restricted to the Bay of Biscay)
F
εNd
P
D
Δ S. FIS
∇ W. Europe
← modern
Pediastrum spp. (x5)
Pre-Quaternary cysts
[10^3 algae/cm^3]
G
MAR (g.cm^{-2}.kyr^{-1})
55°N insol. (W.m^{-2})

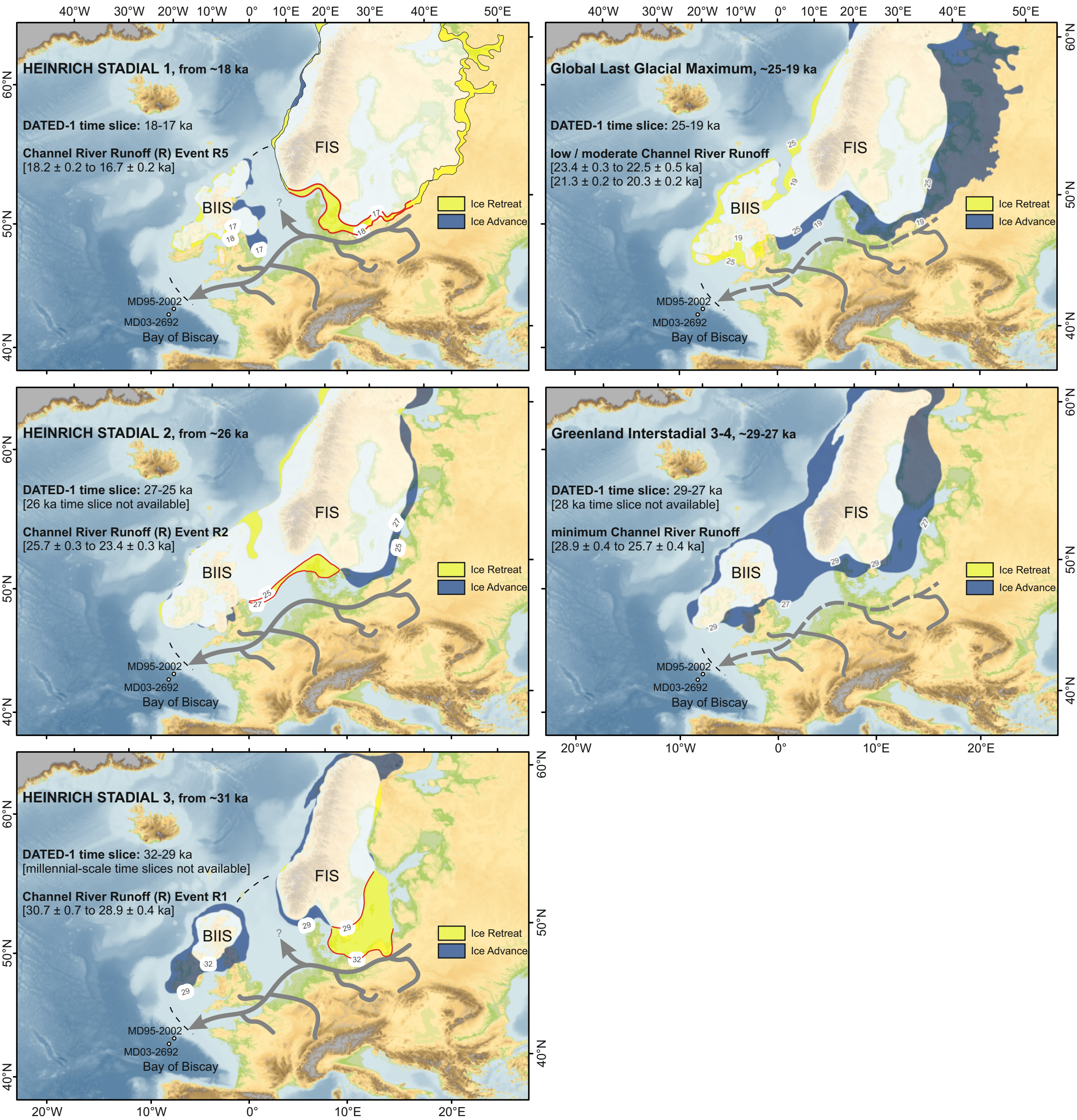
HEINRICH STADIAL 1, from ~18 ka
DATED-1 time slice: 18-17 ka
Channel River Runoff (R) Event R5
[18.2 ± 0.2 to 16.7 ± 0.2 ka]
FIS
BIIS
Ice Retreat
Ice Advance
MD95-2002
MD03-2692
Bay of Biscay
Global Last Glacial Maximum, ~25-19 ka
DATED-1 time slice: 25-19 ka
low / moderate Channel River Runoff
[23.4 ± 0.3 to 22.5 ± 0.5 ka]
[21.3 ± 0.2 to 20.3 ± 0.2 ka]
HEINRICH STADIAL 2, from ~26 ka
DATED-1 time slice: 27-25 ka
[26 ka time slice not available]
Channel River Runoff (R) Event R2
[25.7 ± 0.3 to 23.4 ± 0.3 ka]
Greenland Interstadial 3-4, ~29-27 ka
DATED-1 time slice: 29-27 ka
[28 ka time slice not available]
minimum Channel River Runoff
[28.9 ± 0.4 to 25.7 ± 0.4 ka]
HEINRICH STADIAL 3, from ~31 ka
DATED-1 time slice: 32-29 ka
[millennial-scale time slices not available]
Channel River Runoff (R) Event R1
[30.7 ± 0.7 to 28.9 ± 0.4 ka]
40°W 30°W 20°W 10°W 0° 10°E 20°E 30°E 40°E 50°E
20°W 10°W 0° 10°E 20°E
40°N 50°N 60°N

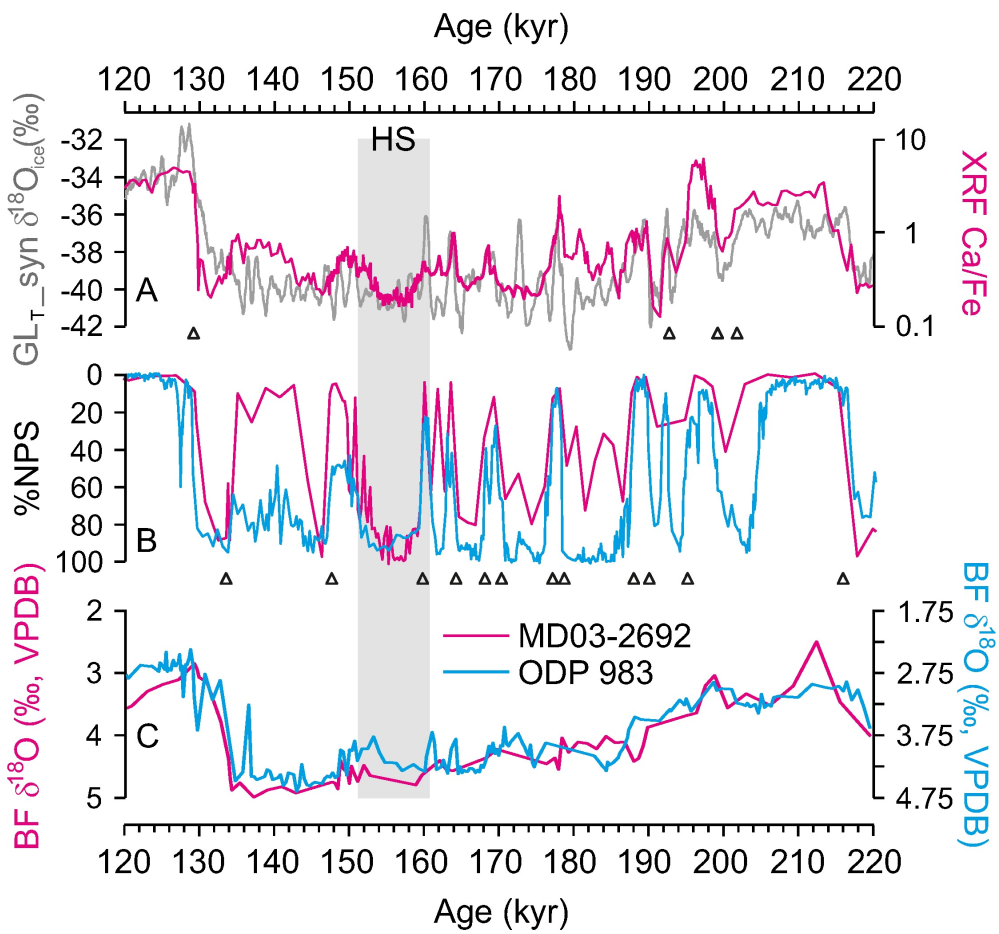

Figure S1. Chronology for MD03-2692. (A) Synthetic Greenland temperatures with orbital components (GL$_T$_syn; Barker et al., 2011) and XRF Ca/Fe for MD03-2692 (Toucanne et al., 2009) are displayed as gray and magenta curves, respectively. (B) Relative abundances of the polar planktic foraminifera *N. pachyderma* (s.) in cores MD03-2692 (magenta, Eynaud et al., 2007) and ODP 983 (blue, Barker et al., 2015). (C) $\delta^{18}O$ of benthic foraminifera from cores MD03-2692 (magenta, Eynaud et al., 2007) and ODP 983 (blue, Barker et al., 2015). Triangles show the tie-points used to construct the chronology for MD03-2692 (see Table S3 for details).

TABLE S1. MD03-2692 SEDIMENTS

Depth (cm)	Age (ka)	$^{143}Nd/^{144}Nd$	±	2 SE	εNd	±	2σ
2023-2024	121.3	0.512033	±	0.000005	-11.8	±	0.3
2035-2036	123.8	0.512029	±	0.000006	-11.9	±	0.3
2051-2052	127.1	0.512048	±	0.000006	-11.5	±	0.3
2083-2084	129.7	0.512024	±	0.000005	-12.0	±	0.3
2093-2094	131.3	0.512019	±	0.000006	-12.1	±	0.3
2111-2112	133.6	0.512021	±	0.000005	-12.0	±	0.3
2145-2146	136.0	0.512036	±	0.000005	-11.7	±	0.3
2157-2158	138.3	0.512033	±	0.000006	-11.8	±	0.3
2165-2166	139.8	0.512046	±	0.000005	-11.5	±	0.3
2189-2190	144.3	0.512034	±	0.000006	-11.8	±	0.3
2201-2202	146.5	0.512037	±	0.000005	-11.7	±	0.3
2259-2260	149.1	0.512062	±	0.000004	-11.2	±	0.3
2333-2334	151.2	0.512051	±	0.000006	-11.5	±	0.3
2373-2374	152.3	0.512039	±	0.000005	-11.7	±	0.3
2395-2396	152.9	0.512034	±	0.000005	-11.8	±	0.3
2429-2430	153.8	0.512007	±	0.000004	-12.3	±	0.3
2461-2462	154.7	0.511939	±	0.000005	-13.6	±	0.3
2493-2494	155.6	0.511918	±	0.000005	-14.0	±	0.3
2507-2508	156.0	0.511944	±	0.000007	-13.5	±	0.3
2527-2528	156.6	0.511952	±	0.000006	-13.4	±	0.3
2559-2560	157.4	0.511958	±	0.000005	-13.3	±	0.3
2577-2578	157.9	0.511989	±	0.000006	-12.7	±	0.3
2611-2612	158.9	0.512035	±	0.000005	-11.8	±	0.3
2641-2642	160.1	0.512049	±	0.000005	-11.5	±	0.3
2653-2654	161.2	0.512046	±	0.000004	-11.6	±	0.3
2663-2664	162.1	0.512045	±	0.000005	-11.6	±	0.3
2673-2674	163.0	0.512025	±	0.000005	-12.0	±	0.3
2685-2686	164.0	0.512053	±	0.000004	-11.4	±	0.3
2697-2698	165.4	0.512051	±	0.000005	-11.5	±	0.3
2703-2704	166.1	0.512051	±	0.000004	-11.4	±	0.3
2717-2718	167.7	0.512029	±	0.000003	-11.9	±	0.3
2725-2726	168.7	0.512043	±	0.000006	-11.6	±	0.3
2735-2736	170.0	0.512039	±	0.000005	-11.7	±	0.3
2739-2740	170.7	0.512047	±	0.000005	-11.5	±	0.3
2747-2748	172.1	0.512055	±	0.000005	-11.4	±	0.3
2767-2768	175.5	0.511989	±	0.000006	-12.7	±	0.3
2771-2772	176.2	0.511981	±	0.000006	-12.8	±	0.3
2799-2800	178.1	0.512082	±	0.000006	-10.8	±	0.3
2817-2818	179.9	0.512059	±	0.000005	-11.3	±	0.3
2825-2826	180.9	0.512053	±	0.000003	-11.4	±	0.3
2839-2840	182.6	0.512043	±	0.000004	-11.6	±	0.3
2855-2856	184.6	0.512056	±	0.000006	-11.3	±	0.3

2867-2868	186.1	0.512049	±	0.000007	-11.5	±	0.3
2891-2892	188.4	0.512050	±	0.000005	-11.5	±	0.3
2913-2914	189.7	0.512038	±	0.000006	-11.7	±	0.3
2923-2924	191.7	0.512017	±	0.000005	-12.1	±	0.3
2927-2928	193.0	0.512030	±	0.000004	-11.9	±	0.3
2929-2930	194.2	0.512019	±	0.000006	-12.1	±	0.3
2943-2944	196.4	0.512044	±	0.000006	-11.6	±	0.3
2953-2954	197.7	0.512040	±	0.000005	-11.7	±	0.3
2967-2968	199.6	0.512054	±	0.000006	-11.4	±	0.3
2973-2974	200.9	0.512034	±	0.000006	-11.8	±	0.3
2985-2986	204.3	0.512061	±	0.000006	-11.3	±	0.3
3001-3002	209.3	0.512051	±	0.000006	-11.5	±	0.3
3013-3014	213.1	0.512054	±	0.000005	-11.4	±	0.3

Table S1. Nd isotope analyses for MIS 6 sediments from core MD03-2692 (Fig. 1). Replicate analyses of the JNdi-1 standard solution (n=31) yield an estimated measurement uncertainty of ±0.3 ε-units (2σ).

TABLE S2. GLACIGENIC SEDIMENTS

Site	ID	Country	Lat. (°N)	Lon. (°E)	$^{143}Nd/^{144}Nd$	±	2 SE	εNd	±	2σ	Sedimentary environment
North European Plain - East (southeastern FIS)								*-14.4*	±	*0.7*	
Szczerców	Sz-461	Poland	51.238	19.165	0.511958	±	0.000005	-13.3	±	0.3	Till, Ławki Fm.
Szczerców	Sz-462	Poland	51.235	19.165	0.511852	±	0.000005	-15.3	±	0.3	Till, Ławki Fm.
Szczerców	Sz-463	Poland	51.235	19.165	0.511961	±	0.000004	-13.2	±	0.3	Till, Ławki Fm.
Szczerców	Sz-464	Poland	51.244	19.163	0.511864	±	0.000004	-15.1	±	0.3	Till, Ławki Fm.
Rogowiec	Rog-1	Poland	51.252	19.154	0.511921	±	0.000005	-14.0	±	0.3	Till, Rogowiec Fm.
Rogowiec	Rog-2	Poland	51.252	19.154	0.511900	±	0.000005	-14.4	±	0.3	Till, Rogowiec Fm.
Rogowiec	Rog-3	Poland	51.252	19.154	0.511906	±	0.000006	-14.3	±	0.3	Till, Rogowiec Fm.
Rogowiec	Rog-4	Poland	51.253	19.154	0.511913	±	0.000007	-14.2	±	0.3	Till, Rogowiec Fm.
Rogowiec	Law-1	Poland	51.253	19.154	0.511872	±	0.000006	-14.9	±	0.3	Till, Ławki Fm.
Rogowiec	Law-2	Poland	51.253	19.154	0.511875	±	0.000004	-14.9	±	0.3	Till, Ławki Fm.
Rogowiec	Law-3	Poland	51.253	19.154	0.511906	±	0.000005	-14.3	±	0.3	Till, Ławki Fm.
North European Plain - West (southwestern FIS)								*-12.4*	±	*0.3*	
Røjle	Røj-5	Denmark	55.552	9.809	0.511997	±	0.000004	-12.5	±	0.3	Till, Palsgård Fm.
Røjle	Røj-10	Denmark	55.552	9.809	0.512017	±	0.000003	-12.1	±	0.3	Till, Trelde Næs Fm.
Røjle	Røj-14	Denmark	55.552	9.809	0.511983	±	0.000003	-12.8	±	0.3	Till, Ashoved Fm.
Trelde Næs	TN-6	Denmark	55.627	9.833	0.511990	±	0.000006	-12.6	±	0.3	Till, Palsgård Fm.
Trelde Næs	TN-16	Denmark	55.627	9.833	0.511993	±	0.000006	-12.6	±	0.3	Till, Trelde Næs Fm.
Ashoved	Ash-2	Denmark	55.745	10.082	0.512025	±	0.000005	-12.0	±	0.3	Till, Palsgård Fm.

Table S2. Geographical information and Nd isotope analyses for the glacigenic sediments (Fig. 1) used to validate the longitudinal variation of εNd in the North European Plain and provide a reference for fingerprinting the provenance of sediments in core MD03-2692 (e.g., Toucanne et al., 2015). Replicate analyses of the JNdi-1 standard solution (n=31) yield an estimated measurement uncertainty of ±0.3 ε-units (2σ). The mean εNd signatures for the Polish and Danish sediments are 14.4 ± 0.7 (n=11) and 12.4 ± 0.3 (n=6), respectively. Sediment stratigraphy is inferred from Houmark-Nielsen (1987) and Kuneš et al. (2013).

TABLE S3. MD03-2692 AGE CONTROL

Depth (cm)	Age (ka)	Tuned parameter(s)
1985	113.3	% *N. pachyderma* (s.)
2060	129.0	Ca/Fe (XRF) vs. GL_T_syn
2105	133.5	% *N. pachyderma* (s.)
2205	147.3	% *N. pachyderma* (s.)
2285	149.9	% *N. pachyderma* (s.)
2635	159.6	% *N. pachyderma* (s.)
2685	164.0	% *N. pachyderma* (s.)
2720	168.0	% *N. pachyderma* (s.)
2735	170.0	% *N. pachyderma* (s.)
2775	176.9	% *N. pachyderma* (s.)
2805	178.4	% *N. pachyderma* (s.)
2880	187.7	% *N. pachyderma* (s.)
2915	189.9	% *N. pachyderma* (s.)
2926	192.4	Ca/Fe (XRF) vs. GL_T_syn
2930	194.9	% *N. pachyderma* (s.)
2964	199.0	Ca/Fe (XRF) vs. GL_T_syn
2976	201.5	Ca/Fe (XRF) vs. GL_T_syn
3025	216.8	% *N. pachyderma* (s.)
3065	224.8	% *N. pachyderma* (s.)

Table S3. Age control points for the MIS 6 chronology of core MD03-2692 were inferred from tuning relative abundances of polar planktic foraminifera *N. pachyderma* (s) to those from the absolutely-dated ODP 983 core (Barker et al., 2011; Toucanne et al., 2009). The chronology was fine-tuned by aligning XRF Ca/Fe ratios of MD03-2692 sediments (Toucanne et al., 2009) with synthetic Greenland temperatures (GL_T_syn; Barker et al., 2011).

TABLE S4. MD03-2692 TERRIGENOUS FLUX

Age (ka)	Mass Accumulation Rate ($g \cdot cm^{-2} \cdot kyr^{-1}$)	Age (ka)	Mass Accumulation Rate ($g \cdot cm^{-2} \cdot kyr^{-1}$)
114	2.43	169	6.01
115	2.13	170	5.68
116	2.08	171	5.26
117	2.19	172	5.42
118	2.19	173	5.45
119	2.15	174	4.96
120	2.07	175	4.28
121	2.17	176	4.29
122	2.26	177	8.04
123	2.15	178	10.05
124	2.09	179	6.87
125	2.08	180	5.27
126	2.11	181	5.28
127	2.14	182	5.24
128	2.18	183	4.98
129	7.71	184	4.69
130	8.22	185	4.73
131	3.40	186	4.71
132	3.54	187	5.07
133	10.20	188	6.84
134	12.11	189	7.93
135	6.38	190	4.98
136	3.18	191	2.26
137	3.23	192	1.88
138	3.19	193	1.24
139	3.19	194	1.02
140	3.15	195	2.25
141	3.11	196	3.39
142	3.31	197	3.48
143	3.60	198	3.87
144	3.69	199	3.42
145	3.53	200	2.66
146	3.44	201	2.23
147	8.29	202	1.70
148	15.84	203	1.35
149	21.06	204	1.35
150	24.27	205	1.35
151	26.08	206	1.38
152	26.00	207	1.46
153	25.35	208	1.46
154	25.33	209	1.46

155	25.72	210	1.48
156	24.72	211	1.54
157	24.77	212	1.60
158	25.83	213	1.61
159	22.00	214	1.72
160	13.60	215	1.89
161	8.22	216	2.10
162	7.81	217	2.81
163	7.64	218	3.51
164	7.73	219	3.59
165	8.00	220	3.55
166	8.05	221	3.59
167	7.41	222	3.60
168	6.36	223	3.42

Table S4. Terrigenous sediment fluxes, quantified as mass accumulation rates (MAR), to the MD03-2692 coring site during MIS 6 (Fig. 2). A 2-kyr moving average was applied to the linearly interpolated (0.1 kyr) MAR data to smooth sharp peaks in the raw data introduced as artifacts of the age model.

SUPPLEMENTARY REFERENCES CITED

Houmark-Nielsen, M., 1987, Pleistocene stratigraphy and glacial history of the central part of Denmark: Bulletin of the Geological Society of Denmark, v. 36, p. 1-189.

Kuneš, P., Kjærsgaard Sørensen, M., Buylaert, J.P., Murray, A.S., Houmark-Nielsen, M., and Odgaard, B.V., 2013, A new Middle Pleistocene interglacial record from Denmark: Chronostratigraphic correlation, palaeovegetation and fire dynamics. Boreas, v. 42, no. 3, p. 596-612, doi: https://doi.org/10.1111/bor.12002